

Towards Autonomous High-Precision Calibration of Digital Cameras

S. Abraham^a and T. Hau^a

^aInstitut of Photogrammetry, Bonn University
Nußallee 15, 53115 Bonn / Germany

ABSTRACT

The demand for high accuracy, for example in 3D-measurements or in quality control, requires high precision calibration of CCD-cameras. In this paper we present a test-field-based high-precision calibration procedure with the focus on the techniques which enable an autonomous calibration: automatic control of the imaging process with geometric tests, algorithms for automatic point detection and matching, automatic determination of approximate values for the orientation parameters and automatic model selection of the interior orientation parameters. Finally, the parameters are estimated in an iterative least squares adjustment.

Keywords: camera calibration, point detection, point matching, minimum description length, bundle adjustment

1. INTRODUCTION

In the last 30 years a large number of different calibration systems and methods have been developed. Camera calibration in photogrammetry originates in aerial photogrammetry. Early presentations of this can be found in^{4,9,14} among others. From these techniques terrestrial procedures were derived: laboratory and test-field calibration procedures^{6,29,30} which use bundle adjustment, too.

In the field of vision applications a variety of different techniques are used, for example: linear and nonlinear methods for modeling the projection, one-stage and two-stage calibrations and non simultaneous and simultaneous calibrations during the measuring task.^{10,22,27} But in many calibration procedures the number of parameters for the interior orientation are reduced to the principle distance, the principle point and two parameters for effects of affinity. For metric applications it is indispensable to use more than these parameters for the interior orientation. Methods which use bundle adjustment show highly accurate results when using additional parameters for modeling the interior orientation.^{3,13} For the interior orientation at least a dozen of different parameter sets were proposed.^{5,9,14,28}

Further investigations, for example special effects of electronic cameras, are presented in.^{3,8,19,21}

Often the degree of automation of the procedures and methods is not very high. In general, the correspondence problem is not solved; the measurement in images works only semi-automatically, and the determination of approximate values for bundle adjustment is a manual procedure. Coded measurement points, which are supplied with point number codes to solve the correspondence problem make automation possible.²³

We present an automatic calibration system which operates on a test-field. For it's target-coordinates only approximate values are necessary. Their specific pattern enables the identification. The test-field is taken from different views. The points are observed in the digital images and are inserted in the bundle adjustment. During the adjustment process, the calibration parameters are defined. The only interaction in the whole process is to turn and rotate the test-field when taking the images. Nothing else has to be done. Especially the critical parts in such a process as the detection of the test-field points, the matching to solve the correspondence problem and the determination of approximate values for the estimation procedure work automatically. The whole calibration procedure is presented with the main view on the critical items.

The following results of different CCD-camera calibrations document the simple use of the system and the high accuracies which can be achieved.

Other author information: Abraham: steffen@ipb.uni-bonn.de; Telephone: +49-228-732908; Hau: hau@ipb.uni-bonn.de; Telephone: +49-228-732900; Fax: +49-228-732712

2. THE CALIBRATION PROCESS

2.1. Structure of the calibration process

In general test-field-based calibration procedures can be divided into two parts: the image processing part for the image measurement including the solution of the correspondence problem and the estimation of the calibration parameters. The different tasks can be seen in figure 1.

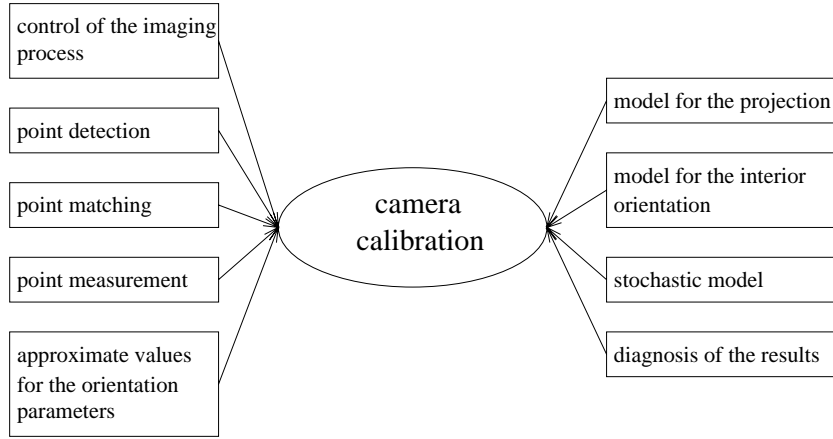


Figure 1. Structure of a calibration tool

Compared to other systems our calibration system includes several new techniques:

- The signalized points of the test-field and the observations in the image plane are matched automatically. The test-field used in our approach is very simple and can be manufactured easily without high precision.
- The approximations for the interior and exterior orientation, which are necessary for the bundle adjustment, are derived without a priori knowledge about the camera.
- The theory of the minimum description length is chosen to find the best model from different parameter sets for the interior orientation.
- One implemented parameter set to describe deviations from the strict central projection is based on Chebyshev polynomials. Since Chebyshev polynomials are normalized, the maximum distortion can be predicted directly.
- Minimum human interaction is required. An operator is only needed to turn the test-field. Full automation with a turning and a rotating tool for the test-field is possible.

2.2. The adjustment process

The modeling of the projection

The projection is represented by the collinearity equation

$${}^k \mathbf{p}_{ij} = \mathbf{R}_j(\omega, \phi, \kappa) (\overset{o}{\mathbf{p}}_i - \overset{o}{\mathbf{p}}_{0j}) \quad (1)$$

$$\overset{b}{\mathbf{p}}_{ij} = \frac{c}{z_{ij}} \begin{pmatrix} {}^k x \\ {}^k y \end{pmatrix}_{ij} \quad (2)$$

which is extended by a polynomial to model deviations from the strict central projection. The extended collinearity equation is

$$\mathbf{p}_{ij}^b - \Delta \mathbf{p}_{ij}^b = \frac{c}{z_{ij}^k} \begin{pmatrix} x \\ y \end{pmatrix}_{ij} \quad (3)$$

with

- $\mathbf{p}_i^k = (x, y, z)_i^k T_i^T$ being the coordinates of the object points P_i in the camera system S_k , which is oriented parallel to the image plane; its origin is the projection center \mathbf{p}_0^o of the camera;
- \mathbf{R}_j is the rotation matrix to rotate the camera system into the object coordinate system S_o ;
- \mathbf{p}_i^o are the point coordinates in the object coordinate system;
- \mathbf{p}_{0j}^o are the coordinates of the projection center in the object coordinate system;
- \mathbf{p}_{ij}^b are the coordinates of the object points in the image coordinate system S_b and
- c is the principle distance, the plane $\mathbf{z} = c$ describes the image plane.

The index i marks the point number, the index j the image number.

For the extension of the parameters of interior orientation $\Delta \mathbf{p}_{ij}^b$, two models are implemented:

1. Chebyshev-polynomial: Chebyshev polynomials are normalized orthogonal polynomials which permit that the corrections on the measured image coordinates can be read immediately from the coefficients of the polynomial because the polynomial is normalized. Furthermore, high correlations between the polynomial coefficients can be avoided in the estimation process. In this way the estimation is more reliable and the convergence of the iterative estimation procedure is improved.

The Chebyshev polynomial for the image coordinates in the image coordinate system is

$$\Delta x_{ij}^b = \sum_{m=0}^M \sum_{n=0}^N a_{mn} T_m(t_x \mathbf{x}_{ij}^b) T_n(t_y \mathbf{y}_{ij}^b) \quad (4)$$

$$\Delta y_{ij}^b = \sum_{m=0}^M \sum_{n=0}^N b_{mn} T_m(t_x \mathbf{x}_{ij}^b) T_n(t_y \mathbf{y}_{ij}^b) \quad (5)$$

with the parameters $T_n(x)$ defined as follows:

$$T_n(x) = \cos(n \arccos(x)) \quad -1 \leq x \leq 1. \quad (6)$$

The parameters t_x and t_y scale the image coordinates to the definition interval $[-1, 1]$.

2. A physically motivated method: The physically motivated method uses different polynomials to describe the deviations from the strict central projection. The coordinate offsets are defined by:

$$\begin{aligned} \Delta x_{ij}^b &= \sum_{k=1}^3 A_k (r_{ij}^{2k} - r_0^{2k}) \mathbf{x}_{ij}^b \\ &+ B_1 (r_{ij}^2 + 2 \mathbf{x}_{ij}^b) + B_2 2 \mathbf{x}_{ij}^b \mathbf{y}_{ij}^b \\ &+ C_1 \mathbf{x}_{ij}^b + C_2 \mathbf{y}_{ij}^b \\ &+ (D_1 (\mathbf{x}_{ij}^b - \mathbf{y}_{ij}^b) + D_2 2 \mathbf{x}_{ij}^b \mathbf{y}_{ij}^b + D_3 (\mathbf{x}_{ij}^b - \mathbf{y}_{ij}^b)) \mathbf{x}_{ij}^b / c \\ &+ \mathbf{x}_H^b \\ \Delta y_{ij}^b &= \sum_{k=1}^3 A_k (r_{ij}^{2k} - r_0^{2k}) \mathbf{y}_{ij}^b \end{aligned} \quad (7)$$

$$\begin{aligned}
& + B_2(r_{ij}^2 + 2 y_{ij}^b) + B_1 2 x_{ij}^b y_{ij}^b \\
& + (D_1(x_{ij}^b - y_{ij}^b) + D_2 2 x_{ij}^b y_{ij}^b + D_3(x_{ij}^b - y_{ij}^b)) y_{ij}^b / c \\
& + y_H^b
\end{aligned} \tag{8}$$

The polynomial for the radial symmetric distortion is described with the coefficients A_k ,²⁸ the radial-asymmetric and tangential distortion is modeled by the parameters B_1 and B_2 .²⁸ Effects of affinity (skew coordinate axes, deviations in the image scale) are taken into consideration by only the x -coordinates with the parameters C_1 and C_2 and global image deformations are described with the parameter D_i .⁵ The parameters x_H^b and y_H^b are the coordinates of the principle point.

Stochastic modeling

The non-linear equation system is solved iteratively with the method of least squares in the Gauß-Markoff model. Its linear formulation is:

$$\mathbf{y} + \mathbf{v} = \mathbf{X}\boldsymbol{\beta} \quad \text{with} \quad D(\mathbf{y}) = \boldsymbol{\Sigma}_{yy} = \sigma_0^2 \mathbf{P}^{-1} \tag{9}$$

where \mathbf{X} is the $n \times u$ design matrix, $\boldsymbol{\beta}$ is the $u \times 1$ vector of the unknown, fixed parameter offsets, \mathbf{y} is the $n \times 1$ vector of the observation offsets, $D(\mathbf{y})$ is the $n \times n$ covariance matrix and \mathbf{P} is the weight matrix.

When using measurements with analogous techniques, correlations between the observation parameters are unknown. The covariance matrix is therefore simplified to $\boldsymbol{\Sigma}_{yy} = \sigma_0^2 \mathbf{I}$. Consequently, only variances can be introduced in most programs. In our bundle adjustment covariances can be introduced, too. It is significant to use correlated observations, especially when using digital measurement techniques.

The unknown parameters are estimated to $\hat{\boldsymbol{\beta}} = (\mathbf{X}'\mathbf{P}\mathbf{X})^{-1}\mathbf{X}'\mathbf{P}\mathbf{y}$. With the vector of observation corrections being $\hat{\mathbf{v}} = \mathbf{X}\hat{\boldsymbol{\beta}} - \mathbf{y}$ the variance of the unit weight is calculated by

$$\hat{\sigma}_0^2 = \frac{\Omega}{n - u} = \frac{\hat{\mathbf{v}}'\mathbf{P}\hat{\mathbf{v}}}{n - u} \tag{10}$$

and so the estimated covariance matrix of the unknown parameters follows as $\hat{\boldsymbol{\Sigma}}_{\hat{\boldsymbol{\beta}}\hat{\boldsymbol{\beta}}} = \hat{\sigma}_0^2(\mathbf{X}'\mathbf{P}\mathbf{X})^{-1}$.

At the end of the estimation procedure gross errors in the observations are removed by data snooping. The criterion for the removal of an observation group is based on a Fisher-test. The test statistic for the i -th observation group, i. e. the i -th point, is

$$T^2 = \frac{\hat{\mathbf{v}}_i^T \boldsymbol{\Sigma}_{\hat{\mathbf{v}}_i \hat{\mathbf{v}}_i}^{-1} \hat{\mathbf{v}}_i}{\hat{\sigma}_0^{(i)2} n_i} \sim F_{n_i, N-u-n_i}, \tag{11}$$

which is Fisher-distributed with n_i and $n - u - n_i$ degrees of freedom. n_i is the number of observations of the i -th observation group and $\boldsymbol{\Sigma}_{\hat{\mathbf{v}}_i \hat{\mathbf{v}}_i}$ is the covariance matrix of the corrections: $\boldsymbol{\Sigma}_{\hat{\mathbf{v}}_i \hat{\mathbf{v}}_i} = (\boldsymbol{\Sigma}_{yy} - \mathbf{X}\hat{\boldsymbol{\Sigma}}_{\hat{\boldsymbol{\beta}}\hat{\boldsymbol{\beta}}}\mathbf{X}')$.

To investigate if the calibration was successful, a simple, rough test value $V = \frac{\hat{\sigma}_0^2}{\sigma_0^2}$ is used. The a-priori variance of unit weight taken from the template matching is compared to the a-posteriori variance. If the model is not correct, both variances will differ and the model will be rejected.

Automatic model selection by MDL

Each camera system has certain properties which can be modeled in different ways. A lot of distortion models have been proposed in the literature. To find the best model automatically an autonomous comparison between different distortion models is desirable. The choice of the adequate model can be based on two different criteria:

- the precision of the adjustment results (covariance matrix) and
- the simplicity of the used model (minimum description length: MDL).

The MDL criterion has been integrated in our system. The description length is based on Coding Theory and is composed assuming that no outliers are present:^{12,26}

$$\begin{aligned}
 D_L &= D_M + D_D \\
 D_L &\text{-total number bits} \\
 D_M &\text{-bits for parameter of the model} \\
 D_D &\text{-bits for data, which are described by the model}
 \end{aligned}
 \tag{12}$$

With the Gauss–Markoff–Model (see eq. 9) and the assumption that the observations are normally distributed the description length can be calculated by:^{7,17}

$$D_L = \frac{u}{2} \log_2(n) + \frac{\Omega}{2 \log_e(2)}
 \tag{13}$$

The principle of MDL states the model with the smallest description length to be the most appropriate. With this criterion we can choose the best fitting model to describe the interior orientation.

2.3. Data acquisition

This part of the calibration is responsible for providing the data for the adjustment process. From the proposals of Godding and Wester-Ebbinghaus^{13,30} a design of the photogrammetric network for the calibration is derived. In this way the system supervises the imaging process. From this network the camera positions are given by the system to the operator. Via image processing the point correspondences, the image coordinates and the orientation parameters of the images are determined. These parameters enable the system to control the geometry of the taken photogrammetric network. With a model–based recognition the unknown parameters of the calibration are derived in the image processing part. Figure 2 gives an overview about the whole process.

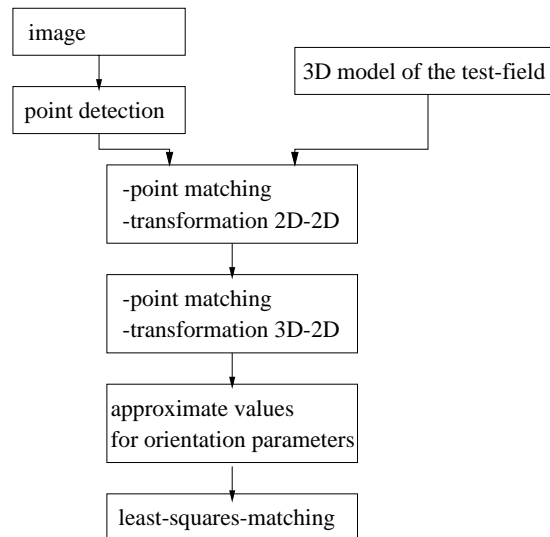


Figure 2. Structure of the image processing

The test-field

In our calibration system a 3D-test-field with dimension of about $700\text{mm} \times 700\text{mm} \times 700\text{mm}$ is used. The field consists of a ground plane with circular retroreflective targets each with a diameter of 25mm . In order to get spatial information some points are arranged on a stamp in front of the plane. The identification process is simplified by a special arrangement of the points in the ground plane (see fig 3).

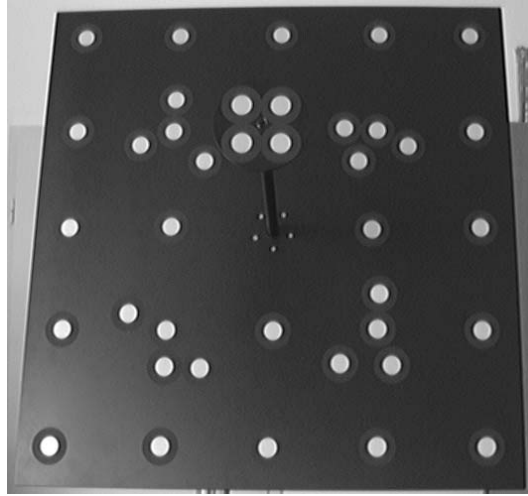


Figure 3. The test-field

Point detection

The retroreflective test-field points are detected in three steps:

1. Object detection:

With a contour algorithm which starts at any local maximum of the image gradient, the contour points are selected. The threshold to find the local maximum is estimated by a histogram. The results of the detection are binary objects.²⁵

2. Preclassification:

In a preclassification every object is checked by different features: closeness of the contour, object area, object circumference and form factor. If the object does not meet one of the criteria, the contour is rejected.

3. Classification:

An adjusted ellipse is defined by an affine normalization.²⁴ The maximal distance of a contour pixel to the adjusted ellipse is limited to one pixel, otherwise the object is rejected as a measurement point. In this way only complete measurement points without occluded parts are used for the estimation process.

Automatic numbering of the points in the ground plane of the test-field

The numbering of the points in the ground plane is achieved by a matching process which also yields a projective transformation between the ground plane and the image plane. In order to simplify and to accelerate the matching process the targets on the test-field are arranged in groups. From the affine normalization the affine projection matrix \mathbf{A}_i between the image plane and the test-field plane is derived. The approximately known ellipse centers $\mathbf{x}_i = (x_i, y_i)^T$ in the image coordinate system S_b can be transformed into the test-field coordinate system S_o . If the radius r of one target is known, the distance between the points \mathbf{x}_j and \mathbf{x}_k

$$d_{jk}(\mathbf{x}_j, \mathbf{x}_k) = r \sqrt{(\mathbf{x}_k - \mathbf{x}_j)^T \mathbf{A}_i^T \mathbf{A}_i (\mathbf{x}_k - \mathbf{x}_j)} \quad (14)$$

can be calculated. With these distances and the knowledge, that the distances within a group are limited to 50mm , the measured points can be divided into groups B_j . From the test-field model the model groups M_i are known. If

the distances within a group B_j are combined in a Matrix $D_j^{(B)}$ and the distances of the model group M_i in the matrix $D_i^{(M)}$ a similarity measure can be realized with a permutation P :

$$\hat{D}_{ij} := \min_P \|D_i^{(M)} - PD_j^{(B)}\|. \quad (15)$$

From the optimal permutation initial values for a 2D-2D projection

$$\begin{aligned} \frac{b}{x} &= \frac{a_{10} + a_{11} \overset{\circ}{x} + a_{12} \overset{\circ}{y}}{1 + a_{01} \overset{\circ}{x} + a_{02} \overset{\circ}{y}} & \frac{b}{y} &= \frac{a_{20} + a_{21} \overset{\circ}{x} + a_{22} \overset{\circ}{y}}{1 + a_{01} \overset{\circ}{x} + a_{02} \overset{\circ}{y}} \end{aligned} \quad (16)$$

between the test-field, assuming $\overset{\circ}{z} = 0$ for the plane points, and the image plane can be defined. First, the transformation parameters are determined with the points of one group. Starting from this first solution the parameters are improved in a robust estimation¹¹ by adding further points.

Automatic numbering of the test-field points on the stamp

In order to identify the targets on the stamp approximate values for the exterior orientation are determined. Assuming the coordinates of the principle point and the Z-coordinates of the plane points of the test-field to be zero, the coefficients of the 2D-2D projection in (16) are identical to the coefficients of the 3D-2D projection in (17).

$$\frac{b}{x} = \frac{a_{10} + a_{11} \overset{\circ}{x} + a_{12} \overset{\circ}{y} + a_{13} \overset{\circ}{z}}{1 + a_{01} \overset{\circ}{x} + a_{02} \overset{\circ}{y} + a_{03} \overset{\circ}{z}} \quad \frac{b}{y} = \frac{a_{20} + a_{21} \overset{\circ}{x} + a_{22} \overset{\circ}{y} + a_{23} \overset{\circ}{z}}{1 + a_{01} \overset{\circ}{x} + a_{02} \overset{\circ}{y} + a_{03} \overset{\circ}{z}} \quad (17)$$

In general the three unknown coefficients a_{13} , a_{23} and a_{03} can be derived by a comparison to the coefficients of the collinearity equation (1) by taking the orthogonality of the rotation matrix into consideration.¹ If the two planes are parallel to each other the coefficients can only be determined with a reasonable assumption for the principle distance.

As the transformation parameters of equation 17 are very weak, model information about the test-field is included in the numbering process for the spatial test-field points.

Approximate orientation parameters

From the resulting transformation parameters the parameters of the interior and exterior orientation can be derived:

- The projection center $\overset{\circ}{p}_0$ is derived from the parameters a_{ik} of the projective projection (17):

$$\begin{pmatrix} a_{11} & a_{12} & a_{13} \\ a_{21} & a_{22} & a_{23} \\ a_{01} & a_{02} & a_{03} \end{pmatrix} \begin{pmatrix} \overset{\circ}{x}_0 \\ \overset{\circ}{y}_0 \\ \overset{\circ}{z}_0 \end{pmatrix} = \begin{pmatrix} -a_{10} \\ -a_{20} \\ -1 \end{pmatrix} \quad (18)$$

- The principle distance c is estimated to be

$$c = \sqrt{\frac{a_{21}^2 + a_{22}^2 + a_{23}^2}{a_{01}^2 + a_{02}^2 + a_{03}^2}}. \quad (19)$$

- The rotation angles ϕ, ω, κ can be calculated by a comparison of the coefficients between the projection matrix (17) and the collinearity equation (1) including the rotation matrix R_j depending on the angles ω, ϕ, κ

$$R_j(\omega, \phi, \kappa) = \begin{pmatrix} \cos \phi \cos \kappa & -\cos \phi \sin \kappa & \sin \phi \\ \cos \omega \sin \kappa + \cos \kappa \sin \phi \sin \omega & \cos \kappa \cos \omega - \sin \kappa \sin \phi \sin \omega & -\cos \phi \sin \omega \\ -\cos \kappa \cos \omega \sin \phi + \sin \kappa \sin \omega & \cos \omega \sin \kappa \sin \phi + \cos \kappa \sin \omega & \cos \phi \cos \omega \end{pmatrix} \quad (20)$$

and the assumption $\overset{b}{(x_H, y_H)} = (0, 0)$:

$$\frac{a_{12}}{a_{11}} = -\frac{\sin \kappa}{\cos \kappa}; \quad \frac{a_{13}}{\sqrt{a_{11}^2 + a_{12}^2}} = \frac{\sin \phi}{\cos \phi}; \quad \frac{1}{c} \cdot \frac{a_{23}}{a_{03}} = \frac{\sin \omega}{\cos \omega} \quad (21)$$

Equation 21 uses the fact that ϕ only can be in the range $[-\pi/2, +\pi/2]$.

Least-squares-matching

At the end of the image processing part of the calibration procedure the image coordinates of the test-field points are measured precisely by a template matching.¹⁶

3. EVALUATION

Calibration results of three different camera systems (table 1) are presented. The distances between camera and test-field were in the range of 1000mm to 1500mm. In the calibration two geometrical configurations were compared: one with 7 different views proposed by Godding¹³ and one with 20 views taken from different views.

	A	B	C
	digital camera Kodak DCS 20	camera: Grundig FA87 grabber: DFG20 optics: Ernitec $f = 8mm$	XC-77CE (Sony) ICP (Imaging Technology Inc) Cosmicar $f = 12.5mm$
image format	493pel \times 373pel	720pel \times 576pel	768pel \times 572pel

Table 1. Camera systems used in the experiments (camera, optics, frame grabber)

Robustness/Reliability of the acquisition step

In our investigation about 500 images were processed. All targets could be detected, because the size of the circles in the images were not too small and the lighting conditions were reasonable. When matching the test-field points only one wrong correspondence occurred. In some configurations the matching process failed (<2%, in most cases on optical systems with high lens-distortion). It seems to be a benefit to integrate a simple distortion model in the matching step, especially for calibration of lenses with high distortions (fish eyes). This is one option for future extension of the matching process. In our system matching failures are detected by the system, the images are rejected and can be taken again. Another simple diagnosis tool in the data acquisition rejects points which are observed only once in the whole photogrammetric network and points which cause a weak geometry by small intersection angles between the projection rays. In all cases, the approximate values calculated in the image processing step were sufficient to reach convergence of the iterative adjustment process within 2-4 iterations.

Selecting the appropriate camera model

In section 2.2. we discussed the MDL as a criterion for selecting an appropriate camera model from a set of models. In our experiments 10 different models (table 2) for describing the interior orientation of a camera were compared. The models are introduced in section 2.2. The numerical results of the MDL criterion are shown in figure 4. The model which was automatically selected is highlighted.

	Chebyshev polynomials (eq. 4)	
tk with k=M=N	$a_{mn}, b_{mn}, M = N = 0, \dots, 7$	0 ... 61
	physically motivated polynomials (eq. 7)	
p1	$\overset{b}{x}_H, \overset{b}{y}_H, A_1, C_1$	4
p2	$\overset{b}{x}_H, \overset{b}{y}_H, A_1, A_2, B_1, B_2, C_1, C_2$	8
p3	$\overset{b}{x}_H, \overset{b}{y}_H, A_1, A_2, A_3, B_1, B_2, C_1, C_2, D_1, D_2, D_3$	12

Table 2. Interior orientation models for automatic model selection

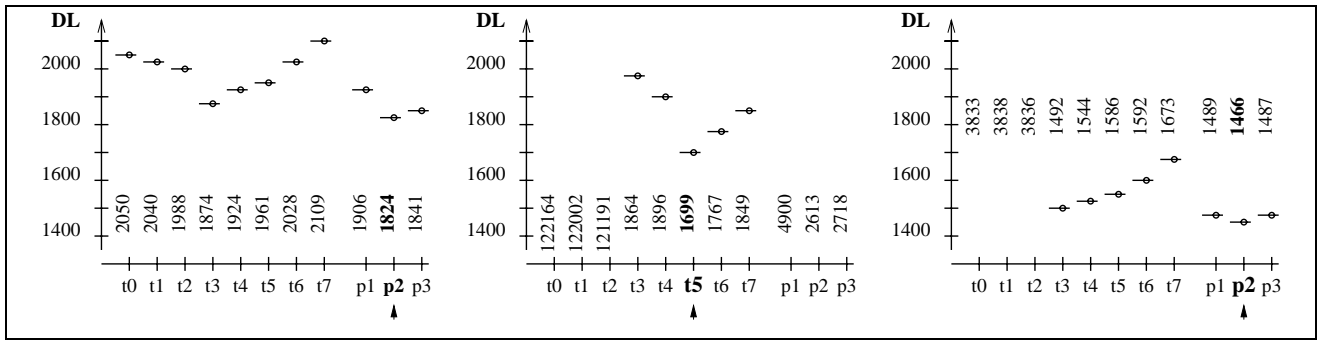


Figure 4. Comparison of different interior orientation models by the MDL criterion for the camera systems **A**, **B**, **C**; highlighted: the selected model

The interior orientation of the camera systems A and C can be well described by the physically motivated distortion model (p2: DL=1824 in A and DL=1466 in C). In system B the physically motivated model (p2: DL=2613) has systematic errors. Model p2 is not sufficient to describe systematic errors of camera B. Better results can be achieved with the Chebyshev polynomial. It can be seen on the residuals (figure 5) and also in the MDL criterion (t5: DL=1699).

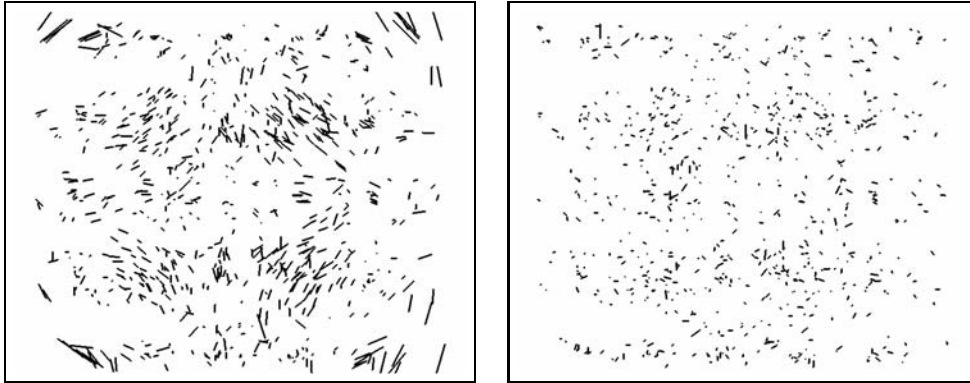


Figure 5. Residuals after calibration of camera system **B**, left side: (model p2, physically motivated), right side (model t5, Chebyshev polynomials), magnified representation of the residuals (**M 100:1**)

Calibration results

Some estimated parameters of the calibration can be found in table 3. Commonly used values to describe the quality of parameter estimations are:

- $\hat{\sigma}_0$: estimated standard deviation of unit weight (precision of observations)
- $RM S_x, RM S_y$: root mean square error between observations and model in the image plain in *pel*
- λ_{max} : upper bound of the standard deviations of the coordinates in object space in *mm* (square-root of largest eigenvalue, comparison between the estimated covariance matrix and the criterion matrix $1mm^2 \cdot \mathbf{I}$ according²)

For demonstration table 3 is extended by the estimated principal distances *c* including their standard deviations. The two geometrical configurations (7 and 20 views) do not show significant differences in the estimated interior orientation parameters. This fact confirms, that the selected model describes the projection process well. The residuals of all image coordinates are shown in figures 5 and 7. Most of the systematic errors are removed. The precision of the estimated parameters can be improved by increasing the number of views in the calibration (comparing 7 and 20 views) as to be expected.

	Views	M_i	$\tilde{\sigma}_0(pel)$	$RMS(pel) \ x y$		$\lambda_{max}(mm)$	$c(pel)$
A	7	(p2)	0.074	0.044	0.073	0.256	675.09 ± 0.86
	20	(p2)	0.079	0.066	0.078	0.175	674.03 ± 0.48
B	7	(t5)	0.050	0.041	0.042	0.272	911.47 ± 0.77
	20	(t5)	0.054	0.041	0.056	0.095	909.21 ± 0.12
C	7	(p2)	0.038	0.033	0.030	0.054	1144.05 ± 0.35
	20	(p2)	0.046	0.037	0.046	0.028	1143.97 ± 0.22

Table 3. Some results from calibration of the three camera systems with 7 and 20 views

The suitability of the three camera systems for measurement tasks can be compared using the precision of the 3D-reconstruction (λ_{max}). As expected camera system **A** has the lowest precision. In contrast to camera **A** system **C** has the highest precision.

According to the selected models the estimated lens distortion is plotted in figure 6. The different scales in the plot show the different properties of the optics.

With the Chebyshev polynomial the upper bounds of the distortions can be determined from its coefficients immediately. The results are presented in table 4.

	A	B	C
$\Delta \overset{b}{x}_{max} [pel]$	0,49	14,71	1,86
$\Delta \overset{b}{y}_{max} [pel]$	0,55	14,30	1,69

Table 4. Upper bounds of the distortions for the three camera systems determined with the coefficients of the Chebyshev polynomial

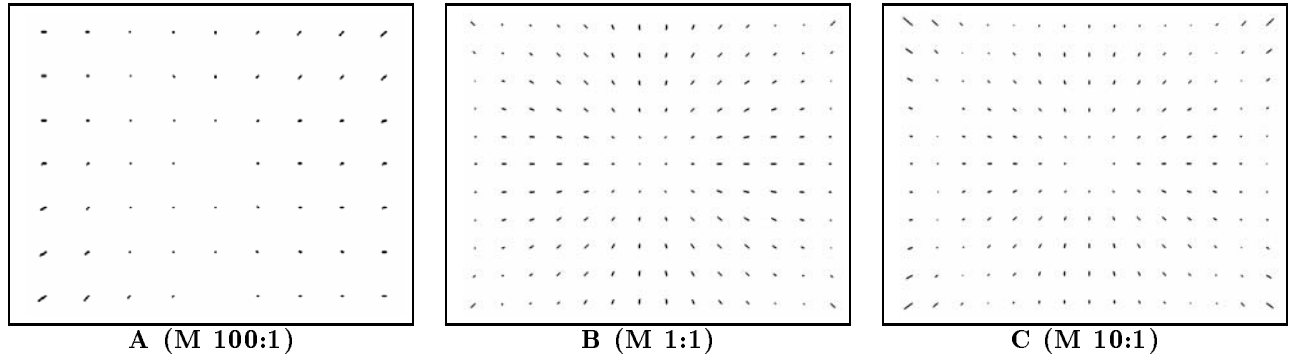


Figure 6. Distortions of camera systems **A**, **B**, **C**, distortions of **A** and **C** are enlarged represented.

Comparison to other systems

A comparison of our results to the accuracy reported in publications is a difficult task. The accuracy measurements depend on various factors: experimental setup, geometrical arrangement, distance between object and camera, etc.. Despite this fact some special items are compared.

The empirical variance of the unit weight $\tilde{\sigma}_0$ is a measure for the precision of the point localization in the image plain. The precision of the LSM algorithm used in our system are in a similar range as results of different point operators.²⁰

The accuracies in the image coordinates (RMS) from high precision calibration in close range photogrammetry ($RMS = 0.018...0.031pel^{13}$) are only a small quantity better than our experimental results. This can be explained

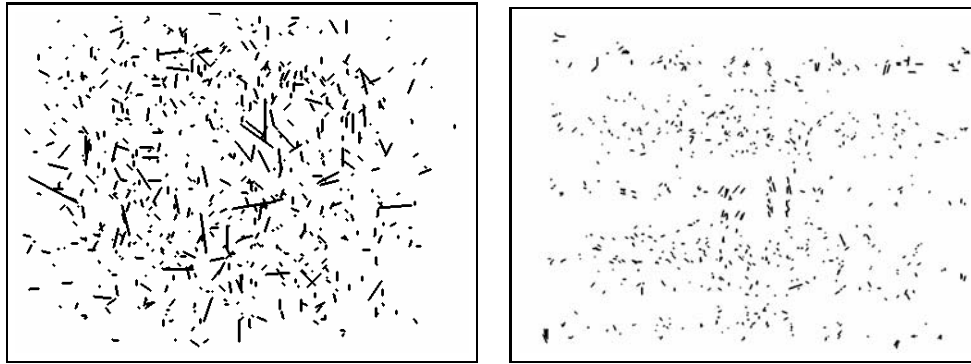


Figure 7. Residuals of camera systems A, C, (magnified representation: M 100:1)

by the special equipment and conditions they had. In comparison to calibration methods reported in computer vision literature our system achieved similar results (for example $RMS = 0.03...0.06pel$,¹⁸ $RMS = 0.1pel$ ¹⁵).

4. CONCLUSION

We presented a calibration system for digital cameras including data acquisition, diagnosis of the data and final adjustment of the parameters. No knowledge about the parameters of the camera is required. The imaging process is supervised by the system whereby the geometric configuration is checked and so the stability in the bundle adjustment is achieved. The whole calibration works automatically up to the human interaction to move the test-field and can be done by unskilled staff.

For future works some improvements of the calibration system are planned. To calibrate wide-angle lenses (fish eyes) the automatic matching process will be extended by a simple radial symmetric distortion model. The distance dependence of the distortion will be modeled so that the calibrated camera can be used in other applications with different projection distances too. To evaluate the results some statistical tests have to be implemented, for example to find systematic effects as drifts in the interior orientation of a camera system. To get a final decision the inner and outer reliability of the estimated parameters have to be defined.

In a new project we are interested in online metric self-calibration from real image sequences without knowledge about the imaged environment. With a diagnosis tool the system should answer the questions dependent on the available data: Which parameters could be calibrated? Which precision can be expected?

REFERENCES

1. S. Abraham and T. Hau. Automatic Camera Calibration. Technical report, Institut für Photogrammetrie, Bonn University, 1997.
2. W. Baarda. *S-Transformations and Criterion Matrices*, volume 5 of 1. Netherlands Geodetic Commission, 1973.
3. H. A. Beyer. *Geometric and Radiometric Analysis of a CCD-Camera Based Photogrammetric Close-Range System*. PhD thesis, Institut für Geodäsie und Photogrammetrie der ETH Zürich, 1992.
4. D. C. Brown. Decentering distortion of lenses. *Photogrammetric Engineering*, pages 444–462, 1966.
5. D. C. Brown. The bundle adjustment - progress and prospects. In *XIIIth Congress of the International Society for Photogrammetry*, 1976.
6. D.C. Brown. Close-range camera calibration. *Photogrammetric Engineering*, 37(8):855–866, 1971.
7. A. Brunn, U. Weidner, and W. Förstner. Model-based 2d-shape recovery. In *DAGM Symposium Mustererkennung 1995*, pages 260–268. Springer Verlag, 1995.
8. J. Dähler. Problems in digital image acquisition with CCD cameras. In *ISPRS Intercommission Conference on Fast Processing of Photogrammetric Data*, pages 48–59, 1987.
9. H. Ebner. Self calibrating block adjustment. *Bild- und Luftbildmessung*, pages 128–139, 1976.

10. O. Faugeras. *Three-Dimensional Computer Vision*. MIT – Press, Cambridge, 1993.
11. W. Förstner. A feature based correspondence algorithm for image matching. In *International Archives of Photogrammetry and Remote Sensing*, pages 150–166. Vol. 26-3/3, 1986.
12. W. Förstner. Image analysis techniques for digital photogrammetry. In *Photogrammetrische Woche Stuttgart*, Schriftenreihe des Inst. für Photogrammetrie Stuttgart, Heft 13, 1989.
13. R. Godding. Ein photogrammetrisches Verfahren zur Überprüfung und Kalibrierung digitaler Bildaufnahmesysteme. *Zeitschrift für Photogrammetrie und Fernerkundung (ZPF)*, pages 82–89, 1993.
14. A. Gruen. Die Simultane Kompensation systematischer Fehler mit dem Münchner Bündelprogramm MBOP. In *XIII Congress of the international society for photogrammetry*, 1976.
15. C. T. Huang and O. R. Mitchell. Dynamic camera calibration. In *International Symposium on Computer Vision, Floral Gables, Florida*, pages 169–174, 1995.
16. F. Lang and W. Förstner. Matching techniques. In *Second Course in Digital Photogrammetry*. Landesvermessungsamt NRW, 1995.
17. Y. G. Leclerc. Image partitioning for constructing stable descriptions. In *Image Understanding Workshop, Cambridge*, 1988.
18. R. Lenz. Lens distortion corrected CCD-camera calibration with co-planar calibration points for real-time 3d measurements. In *Fast Processing of Photogrammetric Data*. ISPRS Intercommission Conference, 1987.
19. R. Lenz. Zur Genauigkeit der Videometrie mit CCD-Sensoren. In *Informatik-Fachberichte 180, Mustererkennung*, pages 179–189. DAGM, 1988.
20. T. Luhmann. Results of the german comparison test for digital point operators. In *International Archives of Photogrammetry and Remote Sensing*, volume XXXI of Part B5, Vienna. ISPRS, 1996.
21. T. Luhmann and W. Wester-Ebbinghaus. On geometric calibration of digitized video images of CCD arrays. In *ISPRS Intercommission Conference on Fast Processing of Photogrammetric Data*, pages 35–47, 1987.
22. R. Y. Tsai. An efficient and accurate camera calibration technique for 3D machine vision. In *roceedings, CVPR '86 (IEEE Computer Society Conference on Computer Vision and Pattern Recognition, Miami Beach, FL, June 22–26, 1986)*, 1986.
23. F. A. van den Heuvel. Automated 3-D measurement with the DCS200 digital camera. In A. Gruen and H. Kahmen, editors, *Optical 3-D Measurement Techniques II*, pages 63–71, 1993.
24. K. Voss and H. Suesse. Invariant fitting of planar objects by primitives. *IEEE Transactions on Pattern Analysis and Machine Intelligence*, 19(1):80–84, 1997.
25. K. Voss and H. Süße. *Praktische Bildverarbeitung*. Hanser Studienbücher der Informatik, 1991.
26. U. Weidner. *Gebäudeerfassung aus digitalen Oberflächenmodellen*. PhD thesis, Institut für Photogrammetrie, Universität Bonn, 1997.
27. J. Weng, P. Cohen, and M. Herniou. Camera calibration with distortion models and accuracy evaluation. *IEEE PAMI*, 14(10):965–980, 1992.
28. W. Wester-Ebbinghaus. Photographisch-numerische Bestimmung der geometrischen Abbildungseigenschaften eines optischen Systems. *Optik*, 55(3):253–259, 1980.
29. W. Wester-Ebbinghaus. *Zur Verfahrensentwicklung in der Nahbereichsphotogrammetrie*. PhD thesis, Universität Bonn, 1981.
30. W. Wester-Ebbinghaus. *Einzelstandpunkt-Selbstkalibrierung - ein Beitrag zur Feldkalibrierung von Aufnahmekammern*. DGK, Reihe C, Nr. 289. Universität Bonn, 1983.

ACKNOWLEDGEMENTS

We would like to thank the Robert Bosch GmbH for the support of this project.